On sampling the ocean using underwater gliders

Daniel L. Rudnick[1] and Sylvia T. Cole[1]

Received 29 November 2010; revised 25 April 2011; accepted 1 June 2011; published 6 August 2011.

[1] The sampling characteristics of an underwater glider are addressed through comparison with contemporaneous measurements from a ship survey using a towed vehicle. The comparison uses the underwater glider Spray and the towed vehicle SeaSoar north of Hawaii along 158°W between 22.75°N and 34.5°N. A Spray dive from the surface to 1000 m and back took 5.6 h and covered 5.3 km, resulting in a horizontal speed of 0.26 m s^{-1}. SeaSoar undulated between the surface and 400 m, completing a cycle in 11 min while covering 2.6 km, for a speed of 3.9 m s^{-1}. Adjacent profiles of temperature and salinity are compared between the two platforms to prove that each is accurate. Spray and SeaSoar data are compared through sections, isopycnal spatial series, and wave number spectra. The relative slowness of the glider results in the projection of high-frequency oceanic variability, such as internal waves, onto spatial structure. The projection is caused by Doppler smearing because of finite speed and aliasing due to discrete sampling. The projected variability is apparent in properties measured on depth surfaces or in isopycnal depth. No projected variability is seen in observations of properties on constant density surfaces because internal waves are intrinsically filtered. Wave number spectra suggest that projected variability affects properties at constant depth at wavelengths shorter than 30 km. These results imply that isobaric quantities, like geostrophic shear, are valid at wavelengths longer than 30 km, while isopycnal quantities, like spice, may be analyzed for scales as small as a glider measures.

Citation: Rudnick, D. L., and S. T. Cole (2011), On sampling the ocean using underwater gliders, *J. Geophys. Res.*, *116*, C08010, doi:10.1029/2010JC006849.

1. Introduction

[2] Autonomous underwater gliders [*Davis et al.*, 2003; *Rudnick et al.*, 2004] are being adopted remarkably rapidly by the oceanographic community. Underwater gliders offer the promise of continuous, fine-resolution observations with relatively little need for ship time. Gliders have been used in a variety of applications to date, including observations of eastern boundary currents [*Davis et al.*, 2008], coastal circulation [*Todd et al.*, 2009], an eddy [*Martin et al.*, 2009], and sediment resuspension [*Glenn et al.*, 2008], among many others. The chief limitation of gliders as platforms for ocean sampling is their relatively slow speed through the water. The purpose of this paper is to evaluate glider sampling of horizontal structure in the ocean.

[3] Every method of surveying the ocean projects temporal variability into the horizontal because of the finite time required to complete the survey. This fundamental imperfection has affected every survey of the ocean from the earliest expeditions on ships to modern satellite remote sensing. The essential problem is that the ocean is energetic to very high frequencies, at least up to the buoyancy frequency of several cycles per hour, and even beyond. For example, any survey that is done in some sense slowly relative to the buoyancy frequency would project internal wave variability into spatial variability. A wave number spectrum produced from such a survey would have a contribution from internal waves appearing as variance at some range of wave numbers. The effect of this projection depends on the true variance at these wave numbers, the strength of the internal waves, and details of the sampling.

[4] A program of glider deployments out of Hawaii was undertaken to examine the modulation of thermohaline fine structure in the subtropical gyre. Repeated deployments of the underwater glider Spray [*Sherman et al.*, 2001] (Figure 1) produced a nearly continuous 2.5 year time series of a section along 158°W ending in December 2009. In December 2007, a cruise was undertaken using the towed vehicle SeaSoar [*Pollard*, 1986; *Rudnick and Luyten*, 1996] (Figure 2) with the intent to evaluate glider sampling of horizontal structure. The horizontal speed of Spray was 0.26 m s^{-1}, while that of SeaSoar was 3.9 m s^{-1}, meaning that the effect of projection is very different in the two data sets. Comparing sampling by Spray to that by SeaSoar, which is the closest thing to a "snapshot" currently achieved, shows the effects of this projection.

[5] The paper is organized as follows. Relevant details of the operation and sampling of Spray and SeaSoar are presented. A comparison between adjacent vertical profiles from Spray and SeaSoar demonstrate that the core sensors

[1]Scripps Institution of Oceanography, La Jolla, California, USA.

0148-0227/11/2010JC006849

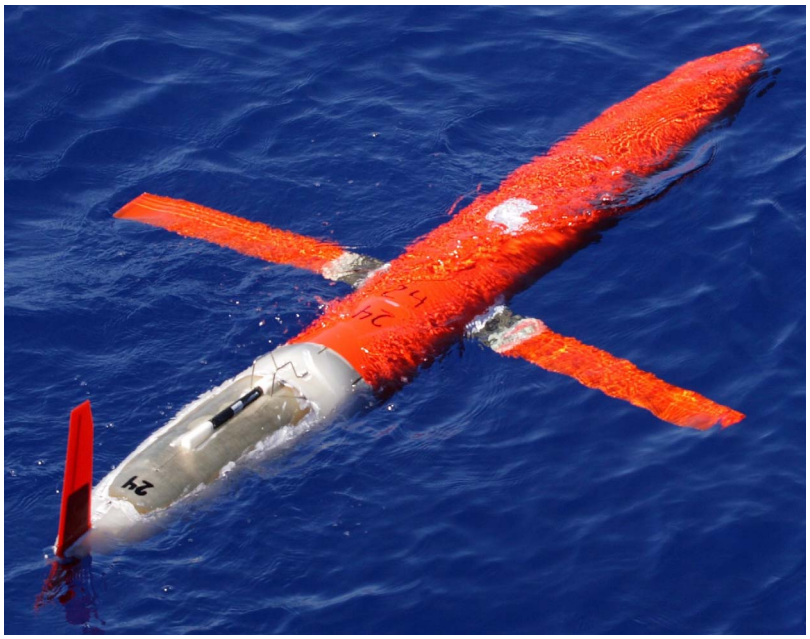

Figure 1. The underwater glider Spray floating at the surface upon deployment. The conductivity cell is the black cylinder on top of the white tail section.

are sufficiently accurate. Observed properties on surfaces of constant depth and potential density, shown as sections and horizontal profiles, provide an initial evaluation of the effects of internal waves. Projection from higher wave numbers and frequencies onto observed wave numbers is shown to be caused by the distinct effects of Doppler smearing and aliasing. Horizontal wave number spectra allow a determination of the length scales at which projection of higher-frequency variability affects the observations. Finally, a conclusion is offered.

2. Data

2.1. Spray

[6] Spray is an autonomous underwater vehicle that profiles vertically by changing buoyancy and flies horizontally on wings [*Sherman et al.*, 2001]. Buoyancy is changed by

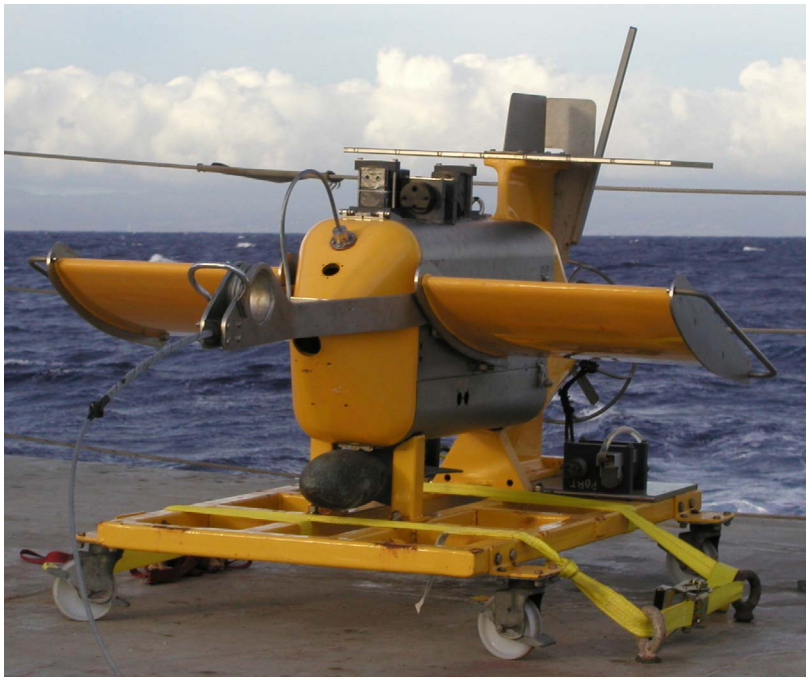

Figure 2. The towed vehicle SeaSoar on the deck of a ship before deployment. The conductivity and temperature sensors are mounted on the lower tail fin facing forward.

Table 1. Summary of Spray Deployments, Including Dates, Northern Latitude, Mean, and Standard Deviation of Dive Displacement and Duration, and Number of Profiles

Deployment Dates	Latitude (deg N)	Δx (km)	Δt (h)	Number of Profiles
3 Jul to 8 Sep 2007	30.0	5.5 ± 1.0	5.6 ± 0.1	290
20 Nov 2007 to 13 Mar 2008	34.5	5.3 ± 0.9	5.6 ± 0.1	492
5 Apr to 7 Jul 2008	31.5	5.3 ± 1.2	6.2 ± 0.2	378
13 Apr to 3 Jul 2008	30.0	5.5 ± 1.2	6.6 ± 0.1	301
4 Aug to 16 Nov 2008	34.5	6.0 ± 1.0	5.7 ± 0.1	440
9 Dec 2008 to 30 Mar 2009	34.5	5.6 ± 0.9	5.8 ± 0.1	466
14 Apr to 9 Aug 2009	34.4	5.2 ± 1.1	5.6 ± 0.1	507
27 Aug to 16 Dec 2009	33.1	5.1 ± 1.0	5.9 ± 0.1	454

pumping hydraulic oil between a reservoir inside a rigid pressure case and an external flexible bladder, in a similar manner as a profiling float [*Davis et al.*, 1992]. There are no movable control surfaces on Spray, so steering is accomplished by changing the glider's internal distribution of mass. One of the battery packs is mounted so that it can be moved fore and aft to adjust pitch, and another battery pack is mounted off axis so that it can be moved side to side to cause roll. Navigation is by the Global Positioning System (GPS), and communication is by the Iridium satellite system. Antennae are located in each of the wings, so Spray executes a 90° roll while on the surface to get a GPS fix, to send data to shore, and to receive commands. The GPS fixes obtained at the beginning and end of each dive allow a dead reckoning estimate of depth-average water velocity. This water velocity is taken into account in the determination of a heading for each dive to reach the desired waypoint. Spray has proven to be reliable, having covered a cumulative distance of over 5 times the earth's circumference during deployments in the global ocean.

[7] Spray deployments off Hawaii were nearly continuous from July 2007 through December 2009 (Table 1). Spray was deployed off the north shore of Oahu, transited to Station Aloha [*Karl and Lukas*, 1996] at 22.75°N, 158°W, and then continued northward along 158°W. The goal was always to reach 34.5°N and return for a total deployment time of 4 months. Contrary currents prevented some of the deployments from reaching this northern goal. Spray dove from the surface to 1000 m, repeating the cycle in an average (over all deployments) of 5.8 h and 5.4 km. During the deployment of November 2007 to March 2008, which overlapped with the SeaSoar cruise, the average dive took 5.6 h and 5.3 km. Standard deviations in cycle time and distance were about 0.1 h and 1 km, within a deployment. Cycle time was largely under operator control during a given deployment, and ballasting causes differences between deployments. Cycle distance over ground was influenced strongly by the depth-average current.

[8] As an example, consider a Spray dive on 8 December 2007 (Figure 3). The dive took 5.5 h from the surface to 1000 m and back, with 2.9 h on descent, and 2.6 h on ascent (Figure 3, left). Glider displacement through the water was estimated using observed pressure, pitch, and heading. Pitch was a nearly constant ±17°, and assuming a constant angle of attack of 3°, the path in Figure 3 (right) was calculated. The assumed angle of attack was the result of hydrodynamic modeling [*Sherman et al.*, 2001] confirmed by analyses of glider performance [*Todd et al.*, 2011]. The dive profile against position (Figure 3, right) was more nearly symmetrical than that against time (Figure 3, left) as pitch was constant, while vertical velocity through the water varied.

2.2. SeaSoar

[9] SeaSoar is a towed undulating vehicle that profiles vertically by changing the angle of attack of its wings.

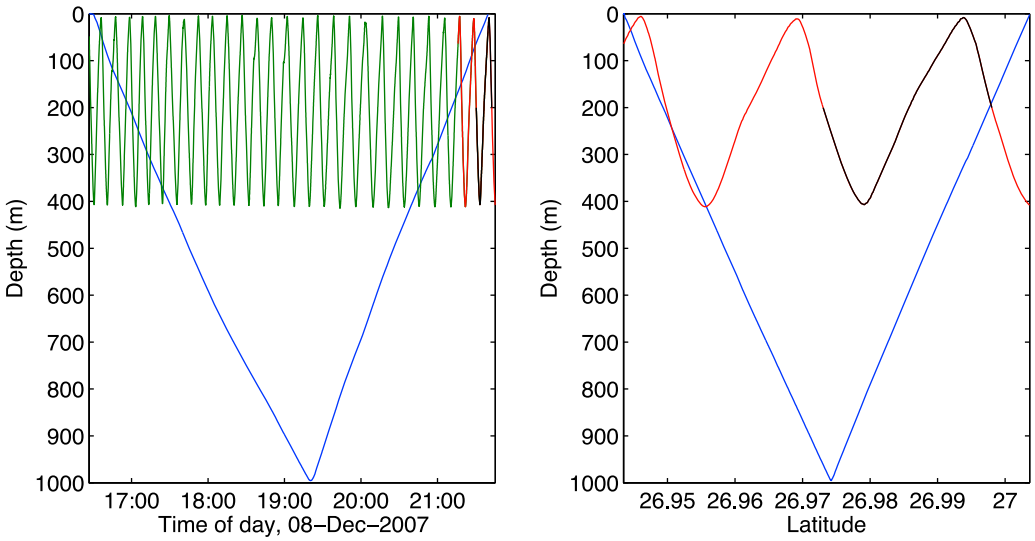

Figure 3. Paths of Spray and SeaSoar during deployments along 158°W north of Hawaii. Paths are shown as functions of depth and (left) time or (right) latitude. A single dive of Spray is shown in blue. The SeaSoar path over the same time range is shown in green, red, and black. Red and black indicate the path covering the same latitude range. A complete dive cycle of SeaSoar (black) is used in comparisons of temperature and salinity measurements with the upward portion of the Spray dive. Note the similarity of (right) the dive slopes of the two platforms and (left) the difference in dive cycle times.

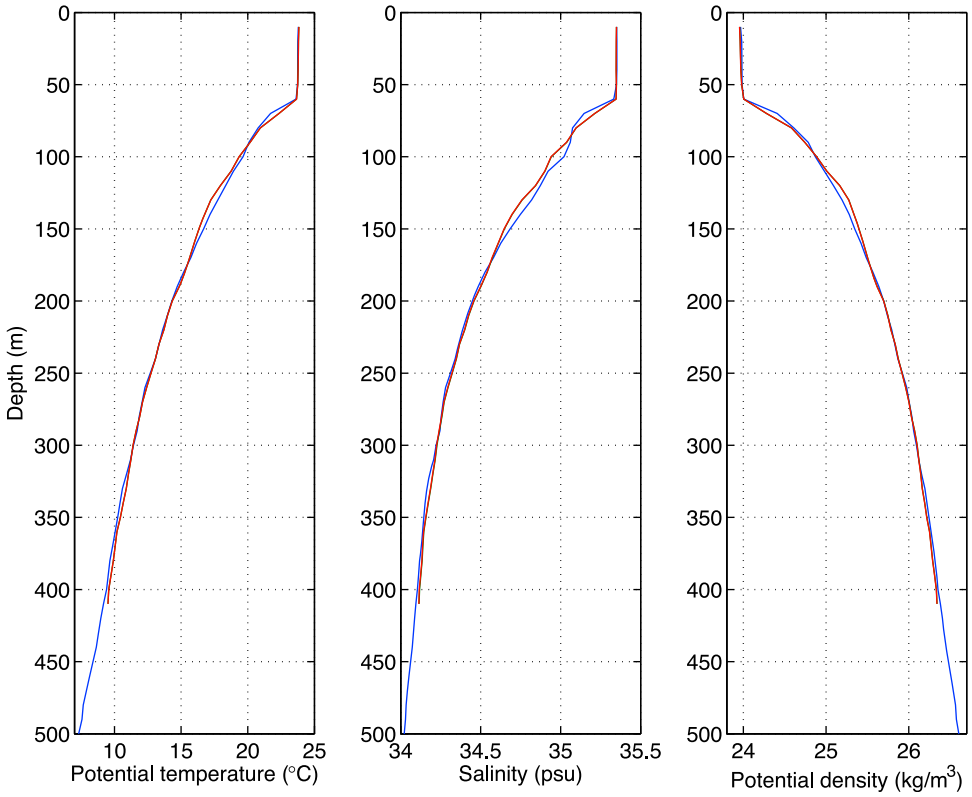

Figure 4. Vertical profiles of potential temperature, salinity, and potential density from Spray (blue) and SeaSoar (red and green, although the differences are so small that only the red line plotted on top is easily discerned). Data are from the upward portion of the Spray profile and black portion of the SeaSoar path in Figure 3, averaged in vertical bins of 10 m.

SeaSoar tow cable is faired to reduce drag and allow deep dives at relatively high tow speeds, and has conductors to allow data transfer and vehicle control. Navigation is by the ship's GPS, and assuming that SeaSoar follows the track of the ship with a fixed time lag. SeaSoar has been in world-wide use for at least 20 years, and its performance remains roughly on par with the range of towed vehicles in current operation.

[10] SeaSoar was used during a cruise on the R/V *Kilo Moana* from 6 to 18 December 2007, following the track along 158°W from Station Aloha to 35°N. SeaSoar was towed in a sawtooth pattern, diving from the surface to 400 m, repeating a cycle in an average of 11 min, and covering an average of 2.6 km, with standard deviations of 1 min and 0.3 km, respectively. SeaSoar was driven to dive and climb as rapidly as possible while keeping the cable tension within safe bounds.

2.3. Comparison

[11] The closest approach of SeaSoar to Spray was on 8 December 2007 (Figure 3). A comparison of depth against time for Spray and SeaSoar (Figure 3, left) demonstrates the difference in the speed of profiling, as 27 SeaSoar cycles were completed during the Spray dive. Interestingly, the dive and climb slopes of Spray and SeaSoar were quite similar (Figure 3, right), and as Spray dove to 1000 m while SeaSoar reached 400 m, more than two complete SeaSoar cycles were completed in the distance covered by one Spray dive. The ship was surveying along 158°W, while Spray was 2.4 km to the east. Spray was on the surface 340 s after finishing a dive when SeaSoar passed the same latitude.

[12] Both SeaSoar and Spray carried conductivity-temperature-depth (CTD) sensors. Spray carried a pumped Sea-Bird 41CP CTD with the sensor mounted on top of the vehicle so that it received clean flow during ascent. Because data quality was superior, and to save power, the CTD was operated only on ascent. SeaSoar carried a Sea-Bird 911+ CTD with two sets of temperature and conductivity sensors, mounted facing forward on the lower tail fin of the vehicle. The SeaSoar CTD sensors were not pumped, relying instead on the dynamic pressure of the 4 m s^{-1} speed through the water to force flow through the sensors. Our experience with both pumped and unpumped sensors on SeaSoar has suggested that unpumped sensors produce reliable results at frequencies lower than 1 Hz.

[13] The closest approach was used to evaluate whether the CTDs on the two platforms reliably produced the same values. CTD data from both Spray and SeaSoar were averaged in 10 m bins, with the shallowest bin centered at 10 m, for the purpose of comparison (Figure 4). One complete cycle (Figure 3, black line) of SeaSoar was used to make the 10 m bins. Profiles from the two CTDs on SeaSoar were so close as to be indistinguishable in this presentation. Differences between Spray and SeaSoar were consistent with internal waves, given the separation in space and time.

[14] A comparison of the potential temperature-salinity (θ-S) relationship from the two platforms is useful, as it filters internal waves (Figure 5). Variations in oceanic

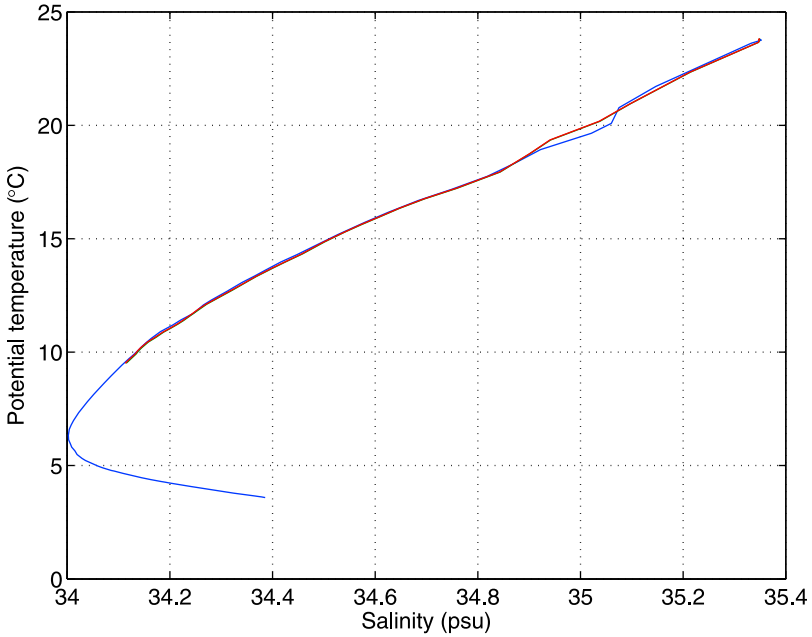

Figure 5. Potential temperature plotted against salinity for Spray (blue) and SeaSoar (red and green). Data are, as in Figure 4, averaged in vertical bins of 10 m.

thermohaline characteristics would be the only reason besides inaccuracies in the sensors for differences in the θ-S relationship. Again, SeaSoar profiles were visually indistinguishable, but there were clear differences between Spray and SeaSoar sensors. The largest differences nearer the surface (19–22°C) were likely due to thermohaline variability. Assuming that the conductivity sensor (as it is sensitive to changes in flow) was most likely to be affected by differences between platforms, salinity was compared in a defined temperature range in deep water. Salinity in the potential temperature range 10–15°C was 34.278 psu for Spray, and 34.281 and 34.279 psu for the two sensors on SeaSoar. On the basis of these comparisons, a reasonable conclusion was that all the sensors were sufficiently accurate.

3. Sections

[15] The archetypical way of looking at a sequence of profiles on a track line is with a section. Thus, a fair question is how to interpret a section by Spray, which takes about 15 times as long to complete as one by SeaSoar. Consider the sections in Figure 6, two of which were done by SeaSoar in 3.8 days each, and one of which was done by Spray in 52.3 days. A casual inspection suggests that the same large-scale field was sampled, with the saltiest water near the surface roughly centered on 27°N, and fresher water at depth. Isopycnals slope upward to the north, and a mixed layer of about 100 m deep is apparent. A closer inspection reveals some differences. The two SeaSoar sections (Figures 6b and 6c) are obviously different at the southern end, which was occupied up to 8 days apart. Changes in salinity and density structure are simply due to oceanic evolution over those 8 days. The biggest differences between Spray and SeaSoar sections (compare Figure 6a with Figures 6b and 6c) are seen at the ends, as the southern end was occupied 2–3 weeks apart, and the northern end was occupied about a month apart. Again, these changes are consistent with oceanic variability, including internal waves and the mesoscale. As discussed above, the closest approach was on 8 December, near 27°N, where essentially the same oceanic structure was sampled.

[16] A striking and important difference between the observations is apparent in isopycnal depth (the black lines in Figure 6), which is more variable at small scales in the Spray section. This variability is a direct result of the relative slowness of Spray, as the temporal variability of internal waves is manifest in spatial variability in observed isopycnal depth. A second difference is that the spatial separation between Spray profiles is about twice that of SeaSoar, so a very close inspection reveals variability at smaller scales in the SeaSoar sections.

4. Isopycnal Thermohaline Variability

[17] It is often valuable to examine thermohaline variability on isopycnals. This thermohaline variability [*Veronis*, 1972; *Jackett and McDougall*, 1985], which by definition does not affect density, has been called "spice" [*Munk*, 1981] because the fluctuations vary from hot and salty to cold and fresh. On the largest scales, the mapping of potential temperature, or equivalently salinity, on isopycnals is used to infer circulation by tracking extrema. On smaller scales, the structure of spice is an expression of how the ocean is stirred in the horizontal. A clear advantage of examining isopycnal thermohaline variability is that internal waves are explicitly filtered. That is, in the absence of diapycnal mixing, thermohaline structure is affected only by processes that advect parallel to isopycnals. We use potential density referenced to the surface to define isopycnals. Nonlinearities in the equation of state may make truly neutral surfaces different from isopycnals [*McDougall*, 1987]. Data considered here are within 400 m of the

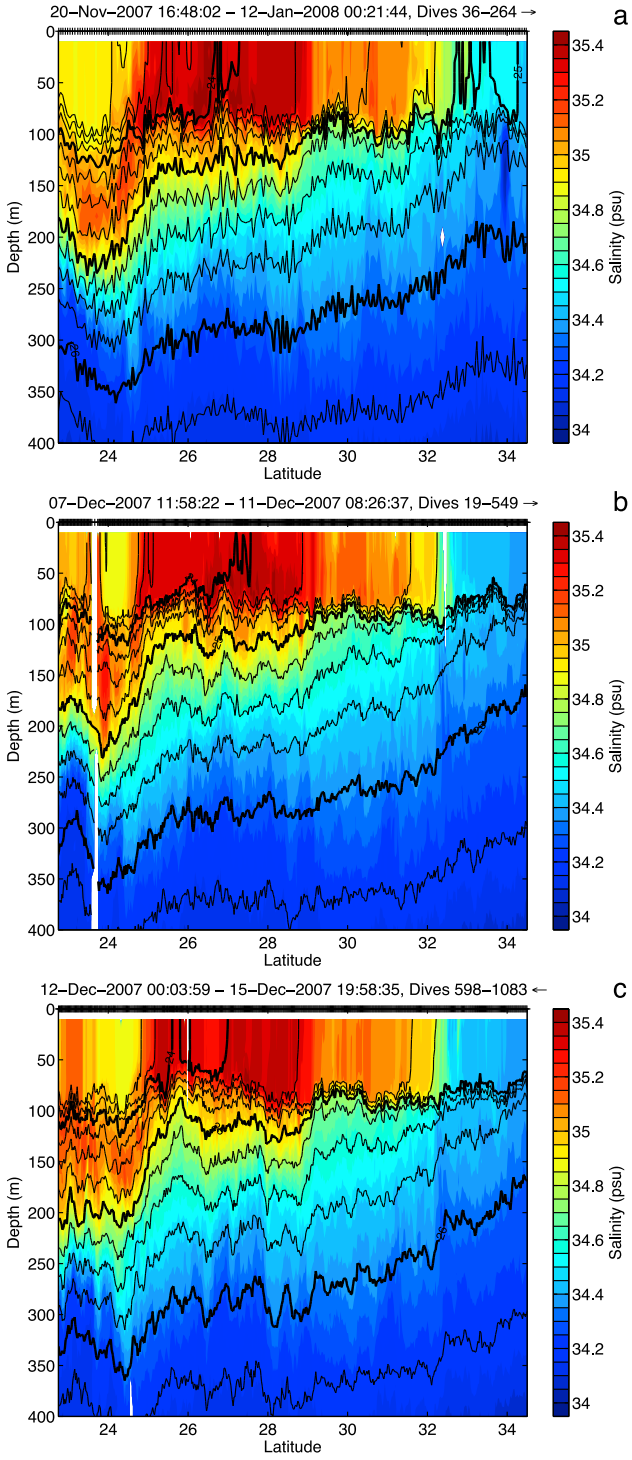

Figure 6. Sections of salinity and potential density plotted as a function of depth and latitude for (a) Spray and (b) northward and (c) southward tows of SeaSoar. Salinity is shown by filled color contours. Isopycnals (black) have a contour interval of 0.25 kg m^{-3} with heavy 24, 25, and 26 kg m^{-3} contours. Tick marks along the upper border of each section mark the locations of profiles. Time intervals, profile numbers, and direction of travel are indicated above each section. Note the similarity of large-scale structure and the enhanced small-scale variability in isopycnal depth in the Spray section (Figure 6a).

surface, so any differences between neutral surfaces and isopycnals are small enough to have negligible effect on the results.

[18] Potential temperature on isopycnals (Figure 7) reveals structure on a range of scales. At the largest scales, there are trends in potential temperature caused by the general circulation. At smaller scales, at least as short as the 3–6 km scales resolved here, the effect of stirring is seen in fluctuations on isopycnals. These fluctuations sometimes extend across a range of isopycnals, with gradients in potential temperature aligned on different isopycnals at the same latitude. Potential temperature on isopycnals observed using Spray has no excess small-scale variability compared to that observed using SeaSoar. This is in direct contrast to observations of isopycnal depth (Figure 6). The explicit filtering of internal waves is responsible for eliminating the noise in Spray measurements of spice.

5. Variability as a Function of Wave Number

5.1. Theoretical Considerations

[19] In any finite speed survey, variability from relatively high frequencies and wave numbers is projected onto variability at observed wave numbers by two distinct effects. The first effect is a Doppler smearing of wave number and frequency. This effect was recognized for towed observations by *Voorhis and Perkins* [1966] and was considered by *Garrett and Munk* [1972] in the first exposition of the internal wave spectrum. The second effect is aliasing [*Bendat and Piersol*, 1986], caused by discrete sampling, leading to variability at higher wave numbers and frequencies being folded into lower wave numbers. The theoretical background for these two well-known effects is presented in the following.

[20] An understanding of sampling is best achieved by considering a variable's representation as a function of wave number and frequency through Fourier transforms. For example, the relationship between a variable, say potential temperature $\theta(x)$, and its Fourier transform $\tilde{\theta}(k)$ in one dimension is

$$\theta(x) = \int_{-\infty}^{\infty} \tilde{\theta}(k) \exp[i2\pi kx] dk, \tag{1}$$

where x is space and k is wave number in cycles per unit space. Sampling in space and time is understood through the two-dimensional Fourier transform. The relationship between $\theta(x, t)$ and its Fourier transform $\tilde{\theta}(k, f)$ is

$$\theta(x,t) = \int_{-\infty}^{\infty}\int_{-\infty}^{\infty} \tilde{\theta}(k,f) \exp[i2\pi(kx+ft)] dk df, \tag{2}$$

where t is time and f is frequency in cycles per unit time.

[21] Sampling in space on a platform moving at constant speed u implies the relationship between x and t

$$t = \frac{x}{u}, \tag{3}$$

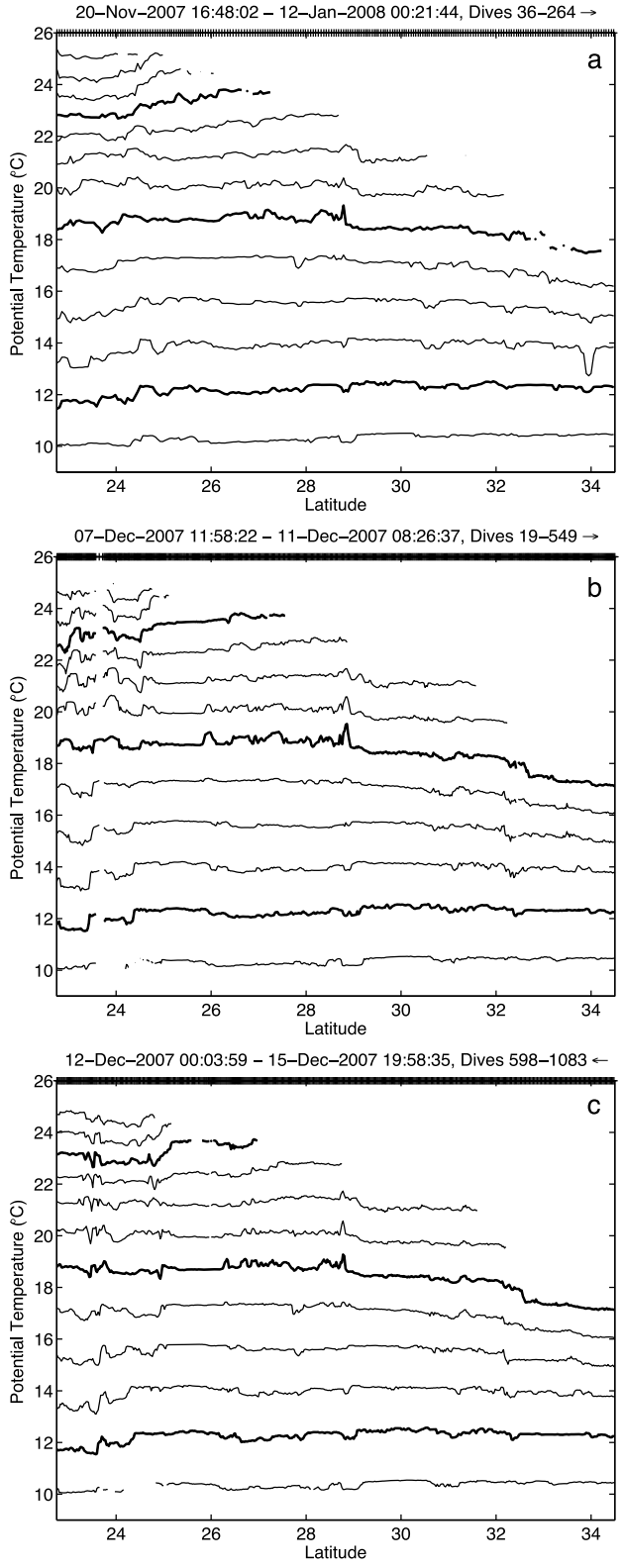

Figure 7. Potential temperature on isopycnals spaced apart by 0.25 kg m^{-3} (with 24, 25, and 26 kg m^{-3} heavy). Tick marks along the upper border of each section mark the locations of profiles. Time intervals, profile numbers, and direction of travel are indicated above each section. Note the similarities in structure at all scales for the two platforms.

so equation (2) becomes

$$\theta(x) = \int_{-\infty}^{\infty}\int_{-\infty}^{\infty} \tilde{\theta}(k,f)\exp\left[i2\pi\left(k+\frac{f}{u}\right)x\right]dkdf. \qquad (4)$$

Comparing equation (4) to equation (1), it is apparent that the Fourier transform at observed wave number $\hat{k}$ has contributions along the line

$$\hat{k} = k + \frac{f}{u}. \qquad (5)$$

Lines of constant $\hat{k}$ in k-f space have slope of $-u$, so that sampling infinitely fast is a vertical slice through all frequencies at a constant wave number. Sampling at finite speed gives contributions to the observed wave number from all wave number-frequency pairs that satisfy equation (5), as sketched in Figure 8. All oceanographic observations of variability from a moving platform smear frequency and wave number in this way. An equivalent to equation (1) is produced by integrating $\tilde{\theta}(k, f)$ along lines of constant $\hat{k}$ to yield $\tilde{\theta}(\hat{k})$.

[22] A second limitation of practical sampling is that individual observations must be discrete in space and time. Given a perfect snapshot in space with resolution Δx, wave numbers higher than the Nyquist wave number $(2\Delta x)^{-1}$ are aliased into lower wave numbers such that the Fourier coefficient at wave number k includes contributions from wave numbers $n\Delta x^{-1}$, where n is an integer. When sampling on a moving platform, the Nyquist wave number is identical, and aliased variability is folded in from lines in the k-f plane, so the Fourier transform at the observed wave number is

$$\tilde{\theta}\left(\hat{k}\right) = \sum_{n=-\infty}^{\infty}\tilde{\theta}\left(k+\frac{f}{u}+\frac{n}{\Delta x}\right), \quad |\hat{k}| < \frac{1}{2\Delta x}. \qquad (6)$$

Smearing wave number and frequency because of surveying at finite speed is understood as occurring on a line of slope $-u$ in the k-f plane, while aliasing because of finite resolution occurs by folding from parallel lines intersecting the k axis at values larger in magnitude than the Nyquist wave number (Figure 8). Because resolution in time is related to that in space by equation (3), there is an equivalent Nyquist frequency.

[23] The effects of smearing wave number and frequency and of aliasing by finite resolution are distinct. That is, by sampling at higher resolution at constant speed, the effect of aliasing can be reduced, but smearing of k and f remains. Sampling infinitely quickly ($u\rightarrow\infty$) eliminates wave number-frequency smearing, but aliasing remains. Neither effect can be unambiguously removed from observations after the fact.

[24] Consider first sampling by SeaSoar. At SeaSoar's mean speed of 3.9 m s^{-1}, and spacing between samples of 2.6 km and 0.18 h, the Nyquist wave number and frequency are 0.19 cycles per kilometer (cpkm) and 2.8 cycles per hour (cph). This frequency is marginally higher than the buoyancy frequency (typically on the order of 1 cph) marking the upper boundary of the internal wave spectrum (except in the region of the mixed layer base). Thus, aliasing from internal waves is nearly absent in SeaSoar data. The lower end of the

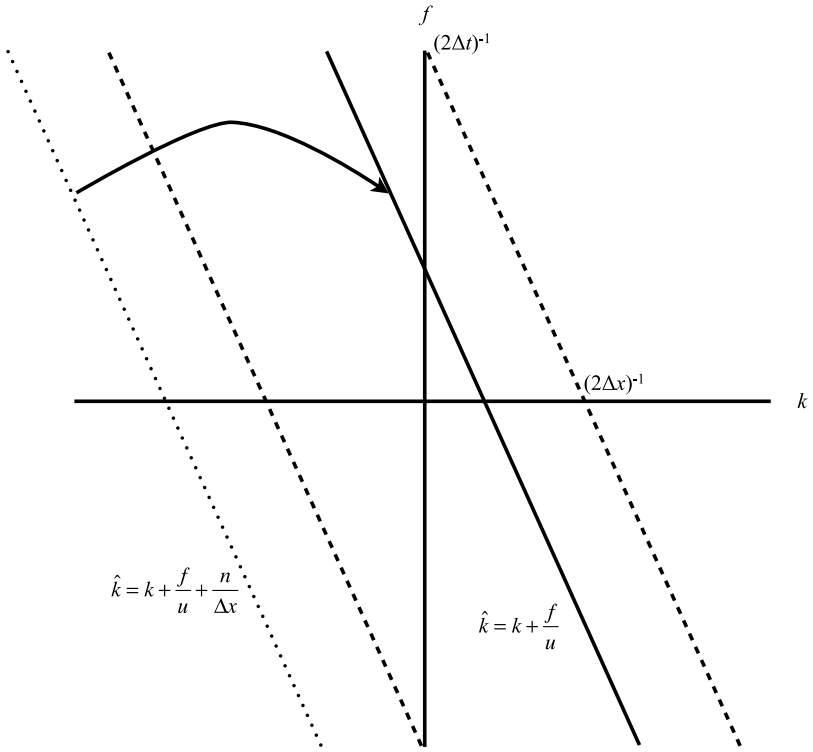

Figure 8. Sampling in the wave number-frequency plane by a moving platform. The line of wave number-frequency pairs Doppler-smeared onto the observed wave number $\hat{k}$ is shown (solid line), as are the lines marking the Nyquist wave number (dashed lines). Aliasing occurs from wave number-frequency pairs higher than Nyquist. One such line is shown (dotted line) for $n = -1$ in equation (6).

internal wave spectrum is at the inertial frequency, 1/24 cph at 30° latitude. Inertial variability at zero wave number would affect the observed wave number of 3.0×10^{-3} cpkm, (a wavelength of about 300 km). Internal waves are smeared in SeaSoar observations.

[25] Consider now sampling by Spray. At Spray's mean speed of 0.26 m s^{-1}, and interval between samples of 5.3 km and 5.6 h, the Nyquist wave number and frequency are 9.4×10^{-2} cpkm and 8.9×10^{-2} cph. The Spray Nyquist frequency is in the middle of the internal wave spectrum. higher-frequency internal waves are aliased, and lower-frequency internal waves are smeared.

5.2. Wave Number Spectra

[26] The smearing and aliasing of internal waves into observations from SeaSoar and Spray is troubling. However, the magnitude of true variability at observed wave numbers also matters. The question of whether, and at what wave numbers, projected internal wave variability exceeds that at lower wave number and frequency requires an examination of observations. This is accomplished through wave number spectra calculated on depth or density surfaces. Results of these calculations reveal the length scales at which glider profiling manifests in false spatial structure.

[27] The calculation of spectra proceeds as follows. As our interest is in length scales of hundreds of kilometers and shorter, Fourier transforms (equation (1)) are done on 650 km chunks of data. The longest sections, extending over 1300 km, contain two such chunks that are averaged, while shorter sections may have one chunk. Because neither Spray nor SeaSoar produces evenly spaced data, observations are interpolated to a regular grid of 0.5 km, a value chosen to be smaller than the typical spacing of either platform. Data are detrended by removing a least squares-fit line, and are tapered to zero at the ends using a 10 km Gaussian window. The spectra are calculated by averaging adjacent frequency bands and then plotted as high as 1/12.5 cpkm, a bit lower than the Nyquist wave number for Spray sampling. The 90% confidence interval is indicated.

[28] Consider spectra of the depth of three isopycnal surfaces (Figure 9). Isopycnal depth is more energetic at low wave number (in analogy with the frequency spectrum of visual light, such spectra are called "red"), consistent with previous observations in the North Pacific subtropical gyre [*Hodges and Rudnick*, 2006; *Cole et al.*, 2010]. A slope of −2 is shown in the log-log plot of spectra, for reference. Concurrent Spray and SeaSoar observations (blue and red lines in Figure 9) yield spectra that agree well up to a wave number of about 0.03 cpkm. At higher wave numbers, projection of high-frequency variability is apparent as the flattening of the Spray spectra (blue and gray lines in Figure 9). The straightforward implication of these spectra is that glider data accurately measures isopycnal depths at wavelengths longer than about 30 km, but is suspect at shorter wavelengths.

[29] The variability of potential temperature at constant depth is affected by internal waves, as the vertical stratification is heaved and tilted. So there are strong similarities between spectra of potential temperature at constant depth in the thermocline (Figures 10b–10d) and spectra of isopycnal

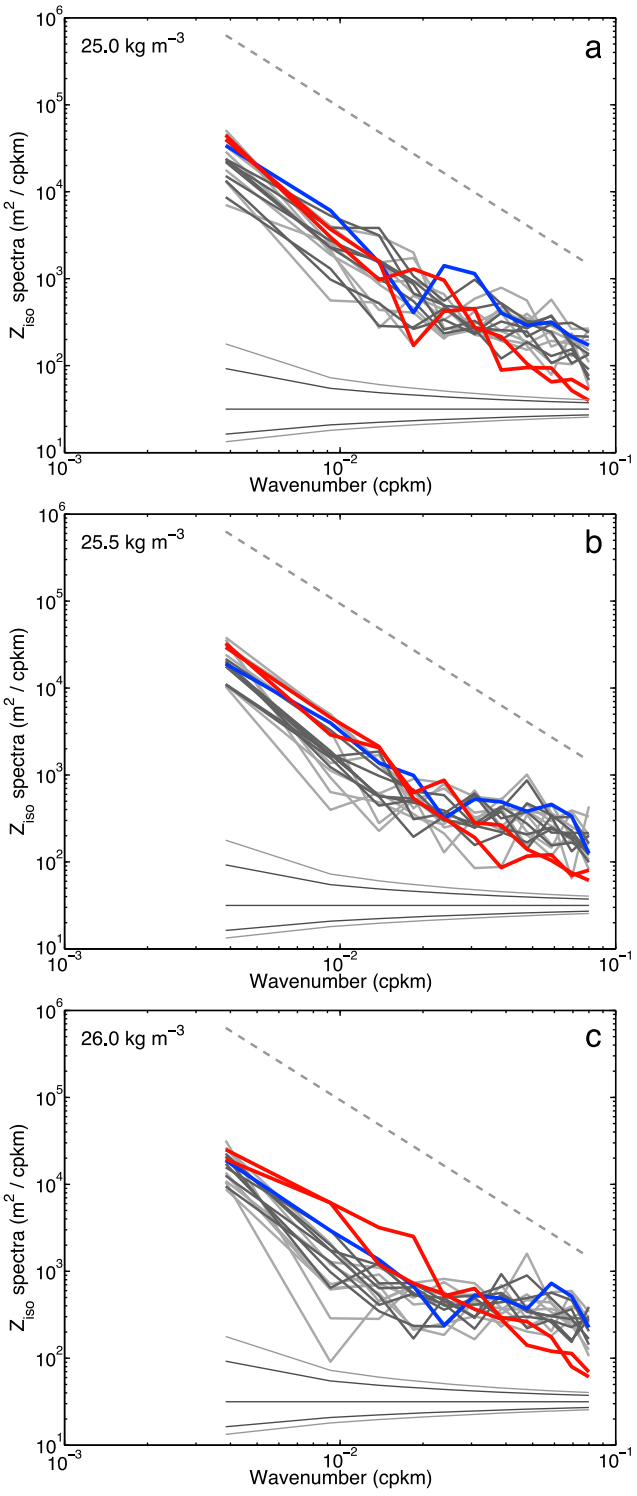

Figure 9. Spectra of depth of the (a) 25.0, (b) 25.5, and (c) 26.0 kg m^{-3} isopycnals as a function of wave number in cycles per kilometer (cpkm). The two SeaSoar sections (red) and concurrent Spray section (blue) are shown. The rest of the Spray deployments are also shown, with sections at least 1300 km long in dark gray and shorter sections in light gray. The 90% confidence intervals are below the spectra for long (dark gray) and short (light gray) deployments, with red and blue spectra being long deployments. The dashed gray line indicates a −2 slope for reference.

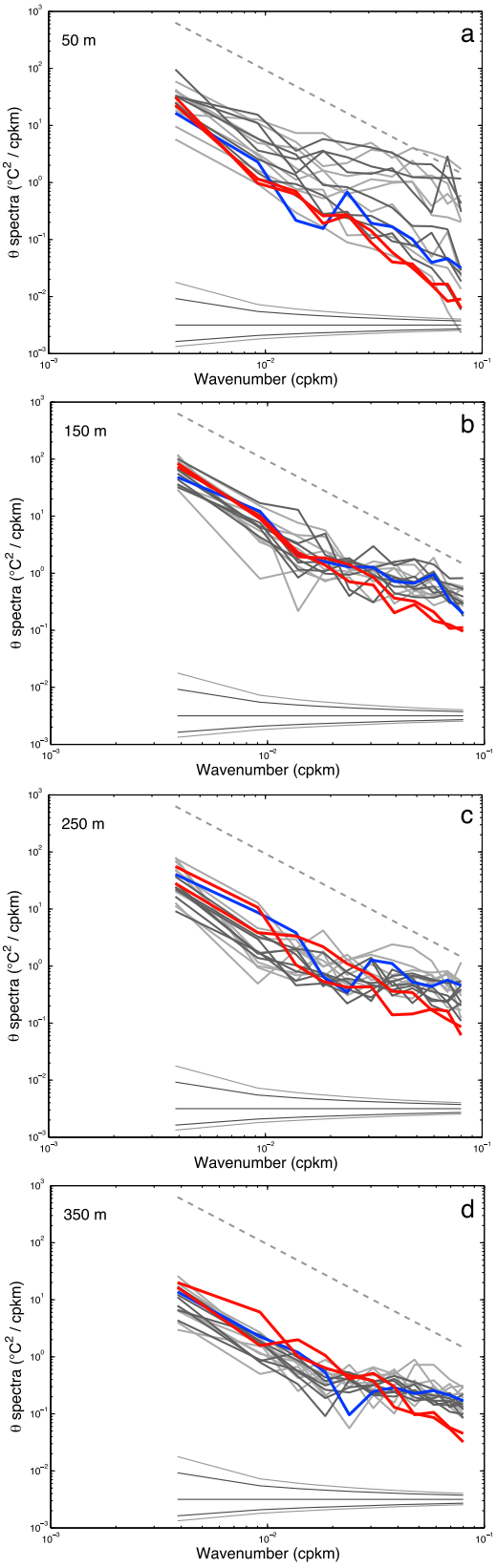

Figure 10. Spectra of potential temperature at (a) 50, (b) 150, (c) 250, and (d) 350 m depth. Lines are the same as in Figure 9.

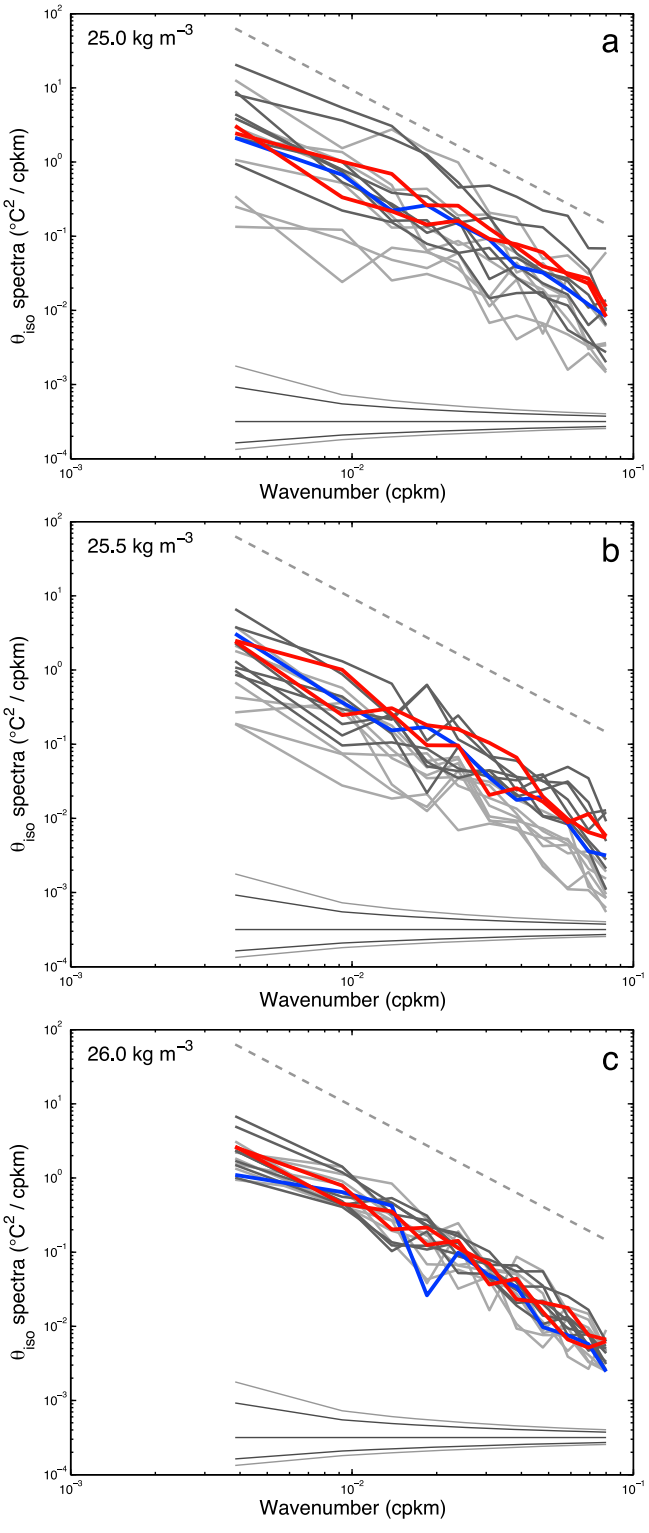

Figure 11. Spectra of potential temperature on the (a) 25.0, (b) 25.5, and (c) 26.0 kg m^{-3} isopycnals. Lines are the same as in Figure 9.

depth (Figure 9). The potential temperature spectra are red at low wave number, with the effect of projection apparent in Spray data above 0.03 cpkm. The magnitudes of the spectra decrease slightly with increasing depth as stratification decreases. This decrease in variance is nearly the same at all wave numbers, so the shape of the spectra does not change much. Apparently, the relative strength of processes that tilt isopycnals is nearly uniform with depth and wave number even as stratification changes. The agreement between concurrent Spray and SeaSoar spectra extends into the mixed layer (Figure 10a) at low wave numbers, with Spray being more energetic at higher wave numbers because of projected variability. The spread among the Spray spectra at 50 m represents seasonal variability, as this depth may be in or beneath the mixed layer depending on the season. The more energetic spectra are from warmer months when the water at 50 m is more stratified.

[30] Spectra of potential temperature at constant potential density from concurrent Spray and SeaSoar observations are remarkably similar throughout the observed wave numbers (red and blue lines in Figure 11). This agreement is a direct consequence of the filtering of internal waves achieved by examining properties on isopycnals. These spectra on constant potential density surfaces are more energetic at lower wave numbers, again consistent with previous observations [*Hodges and Rudnick*, 2006; *Cole et al.*, 2010]. There is some spread in Spray observations at the shallowest displayed isopycnal (25.0 kg m^{-3}; see Figure 11a) as this is near enough to the surface to be influenced by the seasonal cycle. At the 25.5 kg m^{-3} isopycnal, the spectra from longer sections are noticeably more energetic, because spice variance increases to the north (S. T. Cole and D. L. Rudnick, The spatial distribution and annual cycle of upper ocean thermohaline structure, submitted to *Journal of Geophysical Research*, 2011). At the deepest analyzed isopycnal, 26 kg m^{-3}, there is little seasonal or geographic modulation of spice, so all spectra from Spray and SeaSoar coincide. The positive conclusion is that glider data on isopycnals are reliable at all observed wavelengths.

6. Conclusion

[31] The purpose of this article is to compare sampling by the underwater glider Spray, a relatively new technology, to that by the towed vehicle SeaSoar, representative of the most rapid ocean surveying currently achieved. At issue is the relative slowness at which Spray profiles, taking about 6 h to complete a cycle from the surface to 1000 m and back. Our exposition starts by examining the two platforms' flight paths through the ocean. Then adjacent profiles from Spray and SeaSoar are shown to be nearly identical, suggesting that each produces accurate profiles. Sections of properties as a function of depth and horizontal position from either platform yield recognizable large-scale structure, but short-wavelength variability is noticeably stronger in glider observations. This variability is likely attributable to high-frequency (relative to the Spray Nyquist frequency of about 1/12 cycles per hour) variability, such as internal waves, that is projected onto short wavelengths in the section. No such projected variability is apparent in records of properties on isopycnals because of the implicit filtering of internal waves. Spectra of properties at constant depth have a break in slope at a wavelength of about 30 km, providing a length scale above which variability is well resolved.

[32] What are the implications of these results for calculations typically applied to oceanographic sections? Geostrophic shear is calculated from gradients of density at

constant depth. Such a calculation using glider data is sensible at length scales longer than 30 km, but questionable at shorter scales. This limitation to longer scales is not a serious problem as the dynamics leading to a geostrophic balance are appropriate only at these longer scales. It is worth noting that traditional ship surveys where the time between stations is long compared to the buoyancy period have always suffered from a similar problem. Because the distance between ship stations is typically much larger than that between Spray dives, the effect in ship sections has not been as apparent as it is in glider data. Another traditional analysis is to examine temperature and salinity on isopycnals. For such calculations, as of spice, glider data is particularly well suited, especially at the fine horizontal scales gliders can provide. The glider data discussed herein is used in calculation of statistics on constant depth and density surfaces in the work of Cole and Rudnick (submitted manuscript, 2011).

[33] Projection of variability from high wave numbers and frequencies onto resolved wave numbers is caused by two distinct effects. Doppler smearing is produced by the finite speed of the observing platform. Aliasing is a consequence of having discrete samples. Both Spray and SeaSoar operate typically in a relatively narrow range of speeds, so Doppler smearing is an inevitable effect over which the observer has relatively little control. On the other hand, it is easy to trade depth coverage for horizontal resolution by profiling over a reduced range. For example having Spray profile to 500 m, rather than 1000 m, would double the Nyquist wave number and frequency, thus reducing the effect of aliasing. The result would be a shortening of the 30 km wavelength above which variability is resolved. The change in this resolved wavelength depends on the true wave number-frequency spectrum, as smearing remains even as aliasing is reduced.

[34] How might our results from the north Pacific subtropical gyre be extended to glider sampling at other locations? Assuming a Spray operating as described here, the issue has to do with the true oceanic length and time scales. To the extent that there exists a canonical internal wave spectrum [*Garrett and Munk*, 1972, 1975; *Munk*, 1981], high-frequency variability should not vary much in the open ocean away from generation sites. The geographic distribution of low-frequency variability is less well understood, but a general rule is as the ratio of signal (for example, mesoscale) to noise (high frequency internal waves) grows, the resolved wave number is pushed higher. Overall, we anticipate that our results should be typical of other subtropical gyres.

[35] A practical approach to determining the maximum resolved wave number is simply to calculate the wave number spectrum from glider data and find the break in slope. For example, we have done such a calculation using data from the California Current System [*Todd et al.*, 2011] to find a maximum resolved wave number roughly the same as that reported here. In this application, Spray profiles to 500 m in a very energetic coastal environment. We hesitate to suggest that our resolved wavelength of 30 km is universal. Rather we recommend that glider users make a practice of calculating wave number spectra from their data to establish the resolved length scales.

[36] Doppler smearing, like aliasing, is impossible to remove unambiguously after data collection. However, oceanographic surveys have always been plagued with smearing, so there have been many efforts at filtering out projected variability on the basis of assumptions concerning the true variability. For example, using a three-dimensional survey of a front, *Rudnick* [1996] enforced nondivergence in an attempt to isolate the geostrophic velocity field. Tidal variability is often especially strong, which prompted *Candela et al.* [1992] to suggest an analysis method that assumed the true field was made up of spatially varying components only at zero and tidal frequencies. Using a propeller-driven autonomous underwater vehicle whose speed is readily controlled, *Zhang et al.* [2001] advocated sampling different parts of wave number-frequency space by changing speed. These are just a few of many attempts to deal with Doppler smearing. The possible utility of any of these approaches depends on the validity of the underlying assumptions concerning the true oceanographic fields.

[37] Gliders are tools that allow the sustained collection of that most time-honored oceanographic observation, the vertical profile. As profile generating machines, gliders are similar to floats in that they are autonomous, but the positions of the profiles are controllable within limits. Gliders produce sections analogous to those from ships, but their slowness leads to the issues discussed herein at short wavelengths for properties at constant depth. Given gliders' utility, and our growing understanding of their capabilities and limitations, it seems likely that their use will expand in the coming years.

[38] **Acknowledgments.** We are grateful to the Instrument Development Group at Scripps Institution of Oceanography, which was primarily responsible for the success of Spray operations. We thank the captain and crew of the R/V *Kilo Moana* and SIO Shipboard Technical Services, who operated SeaSoar. We acknowledge the National Science Foundation for supporting this work through grant OCE0452574. We thank the anonymous reviewers for helpful comments, especially one reviewer who encouraged a discussion of the Doppler effect.

References

Bendat, J. S., and A. G. Piersol (1986), *Random Data: Analysis and Measurement Procedures*, 2nd ed., 566 pp., John Wiley, New York.

Candela, J., R. C. Beardsley, and R. Limeburner (1992), Separation of tidal and subtidal currents in ship-mounted acoustic Doppler current profiler observations, *J. Geophys. Res.*, *97*, 769–788, doi:10.1029/91JC02569.

Cole, S. T., D. L. Rudnick, and J. A. Colosi (2010), Seasonal evolution of upper-ocean horizontal structure and the remnant mixed layer, *J. Geophys. Res.*, *115*, C04012, doi:10.1029/2009JC005654.

Davis, R. E., D. C. Webb, L. A. Regier, and J. Dufour (1992), The Autonomous Lagrangian Circulation Explorer (ALACE), *J. Atmos. Oceanic Technol.*, *9*, 264–285, doi:10.1175/1520-0426(1992)009<0264:TALCE>2.0.CO;2.

Davis, R. E., C. C. Eriksen, and C. P. Jones (2003), Autonomous buoyancy-driven underwater gliders, in *Technology and Applications of Autonomous Underwater Vehicles*, edited by G. Griffiths, pp. 37–58, Taylor and Francis, London.

Davis, R. E., M. D. Ohman, D. L. Rudnick, J. T. Sherman, and B. Hodges (2008), Glider surveillance of physics and biology in the Southern California current system, *Limnol. Oceanogr.*, *53*, 2151–2168, doi:10.4319/lo.2008.53.5_part_2.2151.

Garrett, C., and W. Munk (1972), Space-time scales of internal waves, *Geophys. Fluid Dyn.*, *3*, 225–264, doi:10.1080/03091927208236082.

Garrett, C., and W. Munk (1975), Space-time scales of internal waves: A progress report, *J. Geophys. Res.*, *80*, 291–297, doi:10.1029/JC080i003p00291.

Glenn, S., C. Jones, M. Twardowski, L. Bowers, J. Kerfoot, J. Kohut, D. Webb, and O. Schofield (2008), Glider observations of sediment resuspension in a Middle Atlantic Bight fall transition storm, *Limnol. Oceanogr.*, *53*, 2180–2196, doi:10.4319/lo.2008.53.5_part_2.2180.

Hodges, B. A., and D. L. Rudnick (2006), Horizontal variability in chlorophyll fluorescence and potential temperature, *Deep Sea Res., Part I*, *53*, 1460–1482, doi:10.1016/j.dsr.2006.06.006.

Jackett, D. R., and T. J. McDougall (1985), An oceanographic variable for the characterization of intrusions and water masses, *Deep Sea Res.*, *32*, 1195–1207, doi:10.1016/0198-0149(85)90003-2.

Karl, D. M., and R. Lukas (1996), The Hawaii Ocean Time-series (HOT) program: Background, rationale and field implementation, *Deep Sea Res., Part II*, *43*, 129–156, doi:10.1016/0967-0645(96)00005-7.

Martin, J. P., C. M. Lee, C. C. Eriksen, C. Ladd, and N. B. Kachel (2009), Glider observations of kinematics in a Gulf of Alaska eddy, *J. Geophys. Res.*, *114*, C12021, doi:10.1029/2008JC005231.

McDougall, T. J. (1987), Neutral surfaces, *J. Phys. Oceanogr.*, *17*, 1950–1964, doi:10.1175/1520-0485(1987)017<1950:NS>2.0.CO;2.

Munk, W. (1981), Internal waves and small-scale processes, in *Evolution of Physical Oceanography*, edited by B. A. Warren and C. Wunsch, pp. 264–291, MIT Press, Cambridge, Mass.

Pollard, R. (1986), Frontal surveys with a towed profiling conductivity/temperature/depth measurement package (SeaSoar), *Nature*, *323*, 433–435, doi:10.1038/323433a0.

Rudnick, D. L. (1996), Intensive surveys of the Azores Front: 2. Inferring the geostrophic and vertical velocity fields, *J. Geophys. Res.*, *101*, 16,291–16,303, doi:10.1029/96JC01144.

Rudnick, D. L., and J. R. Luyten (1996), Intensive surveys of the Azores Front: 1. Tracers and dynamics, *J. Geophys. Res.*, *101*, 923–939, doi:10.1029/95JC02867.

Rudnick, D. L., R. E. Davis, C. C. Eriksen, D. M. Fratantoni, and M. J. Perry (2004), Underwater gliders for ocean research, *Mar. Technol. Soc. J.*, *38*, 73–84, doi:10.4031/002533204787522703.

Sherman, J., R. E. Davis, W. B. Owens, and J. Valdes (2001), The autonomous underwater glider "Spray," *IEEE J. Oceanic Eng.*, *26*, 437–446, doi:10.1109/48.972076.

Todd, R. E., D. L. Rudnick, and R. E. Davis (2009), Monitoring the greater San Pedro Bay region using autonomous underwater gliders during fall of 2006, *J. Geophys. Res.*, *114*, C06001, doi:10.1029/2008JC005086.

Todd, R. E., D. L. Rudnick, M. R. Mazloff, R. E. Davis, and B. D. Cornuelle (2011), Poleward flows in the Southern California Current System: Glider observations and numerical simulation, *J. Geophys. Res.*, *116*, C02026, doi:10.1029/2010JC006536.

Veronis, G. (1972), On properties of seawater defined by temperature, salinity, and pressure, *J. Mar. Res.*, *30*, 227–255.

Voorhis, A. D., and H. T. Perkins (1966), The spatial spectrum of short-wave temperature fluctuations in the near-surface thermocline, *Deep Sea Res.*, *13*, 641–654.

Zhang, Y., A. B. Baggeroer, and J. G. Bellingham (2001), Spectral-feature classification of oceanographic processes using an autonomous underwater vehicle, *IEEE J. Oceanic Eng.*, *26*, 726–741, doi:10.1109/48.972115.

S. T. Cole and D. L. Rudnick, Scripps Institution of Oceanography, La Jolla, CA 92093-0213, USA.